

## Article

# Tuning of Morphology and Surface Properties of Porous Silicones by Chemical Modification

Carmen Racles <sup>1,\*</sup>  and Ana-Lavinia Vasiliu <sup>2</sup> 

<sup>1</sup> Department of Inorganic Polymers, “Petru Poni” Institute of Macromolecular Chemistry, Aleea Gr. Ghica Voda 41A, 700487 Iasi, Romania

<sup>2</sup> Laboratory of Functional Polymers, “Petru Poni” Institute of Macromolecular Chemistry, Aleea Gr. Ghica Voda 41A, 700487 Iasi, Romania

\* Correspondence: raclesc@icmpp.ro; Tel.: +40-232-217-454; Fax: +40-232-211-299

**Abstract:** The behavior of materials against water is a key element in many practical applications. Silicones are hydrophobic by nature and can be chemically modified to become hydrophilic or highly hydrophobic, while combining intrinsic surface properties with morphological details may lead to superhydrophobic materials. Chemically modified porous silicones and their surface properties have rarely been investigated. Our aim in this study was to tune the surface properties of porous silicone materials by a combination of chemical modification and emulsion templating. The porous silicones were obtained by two cross-linking reactions in toluene–water emulsion, in mild conditions: dehydrocoupling of poly(methylhydrogen)siloxane (PMHS) and dimethyl-methylhydrogensiloxane copolymers and UV-initiated thiol-ene addition on a poly(dimethyl-methylvinyl)siloxane, respectively. Apart from the pores generated by water droplets, in the first process, additional large pores appeared due to hydrogen evolution. Their size and number diminished along with the cross-linking degree; thus, the porosity was tuned by adjusting the composition of the reaction mixture. Chemical modifications were performed in situ to introduce more hydrophobic groups (hexane and trimethylsilane) or hydrophilic groups (thioethanol), modifications that were followed by FT-IR spectroscopy. The inner morphology and powder wetting behavior of the crushed samples were investigated by SEM, tensiometry analyses, and contact angle measurements. The materials showed morphological particularities and surface properties that spanned from hydrophilic to superhydrophobic with lotus or petal effects.

**Keywords:** polysiloxanes; emulsion template; dehydrocoupling; thiol-ene photoaddition; superhydrophobic



**Citation:** Racles, C.; Vasiliu, A.-L. Tuning of Morphology and Surface Properties of Porous Silicones by Chemical Modification. *Appl. Sci.* **2023**, *13*, 10899. <https://doi.org/10.3390/app131910899>

Academic Editor: Antonino Pollicino

Received: 14 September 2023

Revised: 28 September 2023

Accepted: 29 September 2023

Published: 30 September 2023



**Copyright:** © 2023 by the authors. Licensee MDPI, Basel, Switzerland. This article is an open access article distributed under the terms and conditions of the Creative Commons Attribution (CC BY) license (<https://creativecommons.org/licenses/by/4.0/>).

## 1. Introduction

Porous polymers have very diverse applications, such as absorption, separation, decontamination, microelectromechanical systems, optical interference coatings, tissue engineering, and (bio)sensing [1,2]. The generation of pores in polymers may be performed by “top-down” approaches, such as nanoimprinting or etching, or by “bottom-up” approaches, which rely on phase separation and block copolymer self-assembly. Methods for producing pores involve the use of porogens in the form of gas, liquid, or solid dispersed phases and combinations of various templates, which leave voids of different sizes after being removed. Other technologies are also used for pore generation, such as electrospinning, 3D printing, freeze drying, or injecting, sometimes combined with template-based ones, aiming to generate hierarchical porous materials.

Silicones, with their most-known representative, polydimethylsiloxane (PDMS), have unique properties, dictated by the particularities of the siloxane bond [3]. PDMS is an insulator and has a low viscosity, a low glass transition temperature (around  $-120$  °C), very low surface tension and pronounced hydrophobicity, good thermal stability, optical transparency, stability to UV and corona discharge, and water vapor permeability. In

addition, silicones are chemically stable, resistant to weathering, have good blood compatibility, and are considered biologically inert. Their chemical modification is possible by various methods and confers special properties and utility to the resultant silicone materials, spanning from liquid crystals and surfactants to electroactive dielectrics [4].

Creating pores in silicones is another way to expand their use, since silicone rubber foams bring together the properties of silicone elastomers and those of foams in materials with low density, heat and cold resistance, good electrical insulation, and biocompatibility [5]. Porous silicones are proposed for applications as sensors [6], sorbents [7], acoustic metamaterials [8], and cell-growth scaffolds [9]. The methods for pore generation in silicones are diverse. The most-known ones rely on crystalline materials with a narrow particle size distribution as sacrificial direct templates [9,10]; employ the emulsion template method, where water droplets act as the porogen [11–13]; or use various foaming agents. The latter can be, for example, supercritical CO<sub>2</sub> [14] or sodium bicarbonate as a CO<sub>2</sub> source [6], alkane by-products in Piers–Rubinsztajn reactions [15], or hydrogen gas. The in situ evolution of hydrogen in dehydrocoupling reactions occurring between Si-H and OH groups in the presence of a platinum catalyst specific for hydrosilylation curing was explored long ago [16]. Additives, such as water, ethanol, ethylene glycol, and 2-methoxyethanol, have been used in order to obtain pores within the membranes, which are possibly useful in ultrafiltration. It was reported that the pore size depends on the additive's reactivity, which controls the rate of H<sub>2</sub> evolution (foam formation). When poly(methylhydrogen)siloxane (PMHS) is crosslinked with a vinyl silicone, pores form due to dehydrocoupling side reactions, and the hydrophilic–hydrophobic properties can be modified [17].

Adjusting the surface properties of polymeric materials is a key aspect for their practical use. For example, foaming issues in the petroleum industry are in close connection to the surface tension and surfactant–polymer interactions [18]. In the biomedical field, the hydrophobic surfaces increase the protein adsorption, which may be undesired in a biological environment, but useful in other applications, like protein separation [17]. Superhydrophobic surfaces have contact angles (CAs) larger than 150°, but an essential parameter that defines their behavior against water is the contact angle hysteresis (CAH) [19]. When the CAH is very low, the surfaces mimic lotus leaves, where water drops roll off [20], and are of interest in self-cleaning coatings, for example. When CAH values are very high, the water drops are pinned on the surface, like in the case of rose petals [21].

Silicones are inherently hydrophobic materials, providing low energy surfaces. Superhydrophobicity can be achieved by chemical modification of silica films or by creating micro-/nanostructures from PDMS using lithography, templates, or chemical reactions, as recently reviewed [22]. For example, a superhydrophobic and oleophobic silicone sponge with hierarchical structures was obtained by introducing a secondary structure on the pore walls of a hydrophobic and oleophilic silicone sponge [23]. Superhydrophobic and superoleophilic behavior was reported for PDMS-MWCNT porous composites, based on the combination of methyl groups on the surface of PDMS and increased surface roughness due to MWCNTs [24]. However, apart from a few exceptions, the literature on porous silicones rarely addresses the surface properties in correlation with chemical structure. On the one hand, assessing the surface properties of porous materials may be challenging, and on the other hand, most porous silicones are designed for specific applications and emphasis is given to their performance. Also, in most articles, the basic materials are commercially available silicone kits, and parameters other than composition or chemical structure are followed.

In our previous report, the emulsion template method was adapted based on a pair of siloxane surfactants soluble in water and in toluene, respectively, and used to obtain porous silicones [13]. In this method, the continuous phase is a solution of silicones in toluene, and the disperse phase is water. The pores are formed by rapid UV-initiated thiol-ene photoaddition reaction, which ensures the cross-linking of the vinyl-containing silicone precursor, followed by the solvent's evaporation.

Herein, the emulsion template method was combined with the dehydrocoupling reaction and chemical modification in order to obtain silicone materials with tunable morphology and surface properties. First, PMHS was cross-linked in emulsion with a Pt catalyst without other additions. Then, the composition of the reaction precursors was varied in order to introduce PDMS segments and lower the cross-linking density. Next, the PMHS was chemically modified in situ with n-hexene or allyltrimethylsilane, aiming to obtain porous materials with increased hydrophobic behavior. In another series, a dimethyl-methylvinyl siloxane copolymer was cross-linked by thiol-ene photoaddition and chemically modified in situ with mercaptoethanol to induce hydrophilic behavior. The resultant materials were investigated in powder state by performing tensiometry wetting measurements, and the obtained results were correlated with qualitative observations and contact angle measurements. Depending on the chemical structure and morphology, the wetting behavior of these materials can span from hydrophilic to superhydrophobic, with “lotus” or “petal” effects. As a consequence, a large diversity of related materials can be obtained by very simple and mild methods, with applications spanning from the sorption of organic compounds to self-cleaning. In particular, the petal effect, observed on three of our samples, and which has rarely been reported in the case of porous silicones, is considered interesting for applications, such as single-molecule spectroscopy and controlled transport of small volumes of liquid in open microfluidic devices [25].

## 2. Experimental Section

### 2.1. Materials and Methods

All reagents and organic solvents were high purity and were used as received: poly(methylhydrogen)siloxane (PMHS) was obtained from Alfa Aesar; Karstedt catalyst, n-hexene, allyltrimethylsilane (ATMS), and trimethylolpropane tris(3-mercaptopropionate) (SHCL) were obtained from Sigma-Aldrich, St. Louis, MO, USA; and 2,2-dimethoxy-2-phenylacetophenone (DMPA) was obtained from Merck. Double-distilled water was used in all experiments.

Poly(dimethyl-methylhydrogen)siloxanes with 10 or 30% Si-H groups (CoSiH10 and CoSiH30) were synthesized according to [26]. A poly(dimethyl-methylvinyl)siloxane copolymer Vi50 with ~50% vinyl groups was obtained by ring-opening copolymerization of octamethylcyclotetrasiloxane ( $D_4$ ) and tetramethyltetravinylcyclotetrasiloxane ( $V_4$ ) according to [27]. The surfactants were prepared as described previously [28].

Fourier transform infrared (FT-IR) spectra were registered on a Bruker Vertex 70 Spectrometer in transmittance mode, in the 400–4000  $\text{cm}^{-1}$  spectral range, with a resolution of 4  $\text{cm}^{-1}$  and an accumulation of 32 scans.

The contact angle was measured by taking digital photos of 10  $\mu\text{L}$  water droplets, following in principle the method described in [29]. Due to the irregular shape and porosity of the broken surfaces that were intended for analysis, attempts to use a goniometer were unsuccessful. Thus, manual adjustments of the sample position, repeated focusing of the camera, and multiple drop (at least 4 for each sample) analysis were carefully performed. The contact angles were measured with ImageJ free software and, alternatively, with the secant method applied manually on enlarged printed images. For each measurement, the average between the left and right CAs was taken, and an average of at least four drops on each sample is reported. Reference materials, like PDMS and glass slides, were measured and a reasonable precision within a few degrees was considered satisfactory for the purpose of our research.

Surface tension and powder wetting measurements were performed with a Sigma 700 automated tensiometer from KSV. All samples were packed in the same way:  $50 \pm 1$  mg of roughly ground material was placed between two filter papers identically cut from the same batch and introduced into a specially designated metallic cylinder with a perforated bottom and a tightly closed piston. The experiments were performed in duplicate for each material, and the results were similar.

SEM investigations were performed with a Quanta 200 microscope (FEI Company, Hillsboro, OR, USA), using an LFD (large field detector), working in low vacuum mode at 20 kV without any coating, and with a Verios G4 UC (Thermo Scientific, Waltham, MA, USA), using an ETD (Everhart–Thornley detector) at 5 kV, for more detailed observation. In the latter case, the samples were coated with 6 nm of platinum with a Leica EM ACE200 sputter coater to provide electrical conductivity and to prevent charge buildup during exposure to the electron beam. All the samples were analyzed in cross sections obtained by breaking the monolith materials.

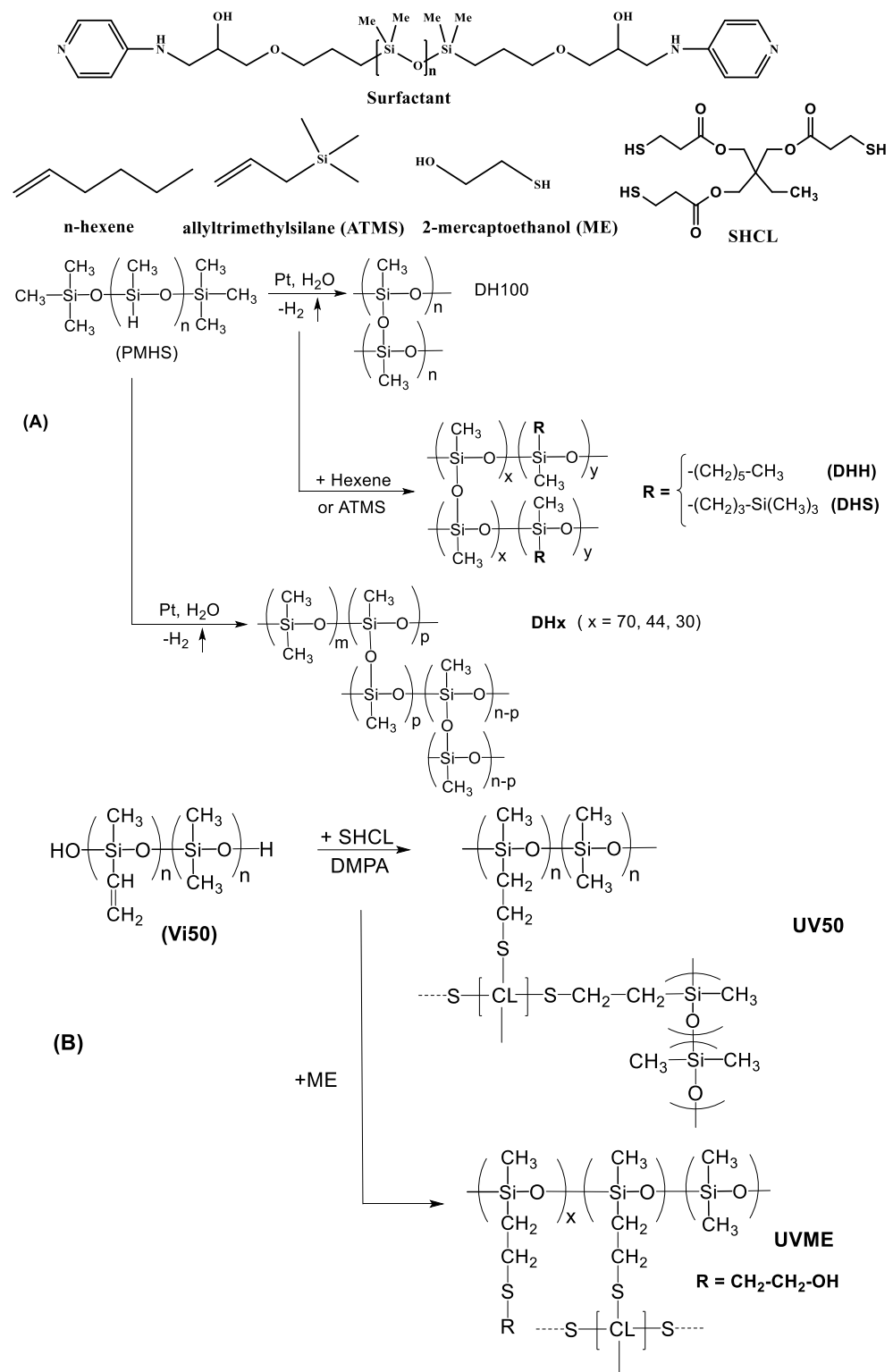
The compression tests were performed using an Instron 3365 two-column universal mechanical testing machine at a 50 mm/min compression rate. Monolith samples of 8 mm diameter were measured in triplicate, and the average value of the Young's modulus at 10% compression was considered.

## 2.2. Preparation of Porous Silicones Cross-Linked by Dehydrocoupling/Hydrosilylation (Series DH)

First, the emulsion template was obtained by mixing 2 mL of a toluene solution containing 1% siloxane oligomer (Scheme 1,  $n=15$ ) with an equal volume of water. After brief manual shaking, the mixture was sonicated for 30 s in a cleaning bath (Elmasonic P, at 37 kHz and 90% power). To the formed emulsion, the polysiloxane precursor was added (please see Table 1 for details) and sonicated for another 30 s, before adding the Karstedt catalyst (1:10 diluted in toluene). The evolution of hydrogen was very quickly observed in the case of DH100, and the cross-linking occurred within 5 min, while for other cases slight heating was necessary. When dimethyl-methylhydrogen siloxane copolymers were used instead of PMHS, a short delay was allowed to increase the hydrolysis rate before adding the catalyst. For chemical modification, PMHS and n-hexene or ATMS were mixed in bulk, then the emulsion was added to the mixture. To ensure hydrosilylation conditions, the amount of catalyst was increased. In certain experiments, the temperature was raised to 50 °C (please see Table 1). The resultant porous materials were dried freely in laboratory ambient conditions for several days. DHH and DHS were washed with ethanol and water and dried again.

**Table 1.** Experimental details for the preparation of the porous materials. The samples codes indicate the method (dehydrocoupling or UV) and the theoretical crosslinking degree or the substituent.

Code	Amount of PMHS, g	Type, Amount of CoSiH <sub>x</sub> , g	Modification Reagent, g	Vi50, g	Catalyst Amount	Reaction Conditions
DH100	0.5	-	-		25 µL	R.T.
DH70	0.33	CoSiH10 (0.17)			25 µL	R.T.
DH44	0.1	CoSiH30 (0.4)			25 µL	R.T.
DH30	-	CoSiH30 (0.5)	-		25 µL	50 °C 1 h, R.T. 1d
DHH	0.5		hexene (0.2)		40 µL	50 °C, 3 h, R.T. 1d
DHS	0.5	-	ATMS (0.25)		40 µL	R.T. 1d
UV50				0.6	50 µL SHCL, 11 mg DMPA	UV, 5 min
UVME			ME (0.2)	0.4	50 µL SHCL, 11 mg DMPA	UV, 5 min



**Scheme 1.** Reagents and cross-linking reactions: **(A)** dehydrocoupling–hydrosilylation and **(B)** thiol-ene addition.

### 2.3. Preparation of Porous Silicones Cross-Linked by Thiol-Ene Photoaddition (Series UV)

The procedure is largely described in our previous paper [13]. Herein, the emulsion was obtained using only one telechelic oligomer with  $n = 15$ , then a poly(dimethylmethylvinyl) siloxane copolymer Vi50 with ~50% vinyl groups was added. After polymer dissolution and a brief sonication, SHCL and DMPA were introduced. The mixture was exposed to UV light for 5 min, and the material (UV50) was allowed to dry freely, washed with water and with ethanol, then dried again at 50 °C.

For the chemical modification, 2-mercaptoethanol (ME) was dissolved in water and the solution was mixed with the toluene surfactant solution containing Vi50 under vigorous mixing to form the emulsion. Then, the catalyst and initiator were added, and the mixture was submitted to UV irradiation. The result was a thick cross-linked film and ca. 1 mL of latex. The film (UVME) was washed thoroughly with water, blotted with filter paper, and left to dry under the hood; then it was extracted with water and ethanol and dried at 50 °C.

## 3. Results and Discussion

The emulsion stabilizer was an in-house prepared telechelic siloxane oligomer with aminopyridyl end groups (Scheme 1,  $n = 15$ , HLB 4.4), which is soluble in toluene. The medium internal phase emulsion ( $f = 0.5$ ) of water in toluene was stable from one day to another, when partial demulsification was observed and re-emulsification was very easily performed with an ultrasonic cleaning bath. The stability of the emulsion at 50 °C was also very good within the timeframe of the reaction, since its appearance remained unchanged (Figure S1). The surface tension of the emulsion was  $25.27 \pm 0.07$  mN/m at room temperature and  $24.43 \pm 0.1$  mN/m at 50 °C (by the Wilhelmy plate method).

The dehydrocoupling reaction of PMHS was used to generate pores in combination with the emulsion template method. This reaction, occurring very fast in the presence of Karstedt catalyst at room temperature in bulk, is accompanied by the evolution of hydrogen gas, due to atmospheric moisture. The first step is the partial hydrolysis of Si-H groups in the precursor PHMS [17], followed by the condensation of Si-H and Si-OH groups. In our case, PMHS was formulated as emulsion, and important volume expansion due to the evolution of hydrogen was instantaneously observed once the Pt catalyst was added. The tight cross-linking by Si-O-Si bridges (Scheme 1A) generated a rigid, rather frail foam, in which unreacted Si-H and Si-OH groups were still present, due to the high reaction rate leading to a high cross-linking density and thus rapidly reduced mobility. These reminiscent functional groups can be observed in the FT-IR spectrum (Figure S2), at  $3440\text{ cm}^{-1}$  (OH),  $2174\text{ cm}^{-1}$  (Si-H), shifted from  $2170\text{ cm}^{-1}$  in PMHS, and around  $910\text{ cm}^{-1}$  (Si(H)CH<sub>3</sub>). The wide polysiloxane (Si-O-Si) band is located at  $1030\text{--}1140\text{ cm}^{-1}$  in PMHS and DH100. Other bands at  $1410\text{ cm}^{-1}$  (asymmetric deformation vibration of the CH<sub>3</sub> group),  $1261\text{ cm}^{-1}$  (symmetric deformation vibration of the CH<sub>3</sub> group), 845, and  $781\text{ cm}^{-1}$  (methyl rocking vibration and Si-C stretching vibration) are characteristic of siloxane compounds [30].

The same reaction was used for preparing several porous silicones (Table 1), varying the amount of Si-H groups, either by using a poly(dimethyl-methylhydrogen)siloxane with 30% Si-H groups (DH30) or by combining PHMS with a copolymer with 10% (DH70) or 30% Si-H groups (DH44). In this way, polydimethylsiloxane (PDMS) chains were introduced, which are known as hydrophobic and ensure a more elastic framework, which is useful for certain applications. The presence of PDMS segments was seen in FT-IR by a narrower polysiloxane band, with peaks at  $1024$  and  $1094\text{ cm}^{-1}$ , a stronger band at  $2968\text{ cm}^{-1}$  (CH<sub>3</sub> asymmetric stretching vibration), and shifted Si-C stretching vibration bands, the strongest one at  $800\text{ cm}^{-1}$  (Figure S2). In Table 2, the theoretical cross-linking degree (CLD) is the proportion of Si-H groups in the reaction mixture. However, since the dehydrocoupling reaction cannot be total, the CLD was calculated from the FT-IR spectrum, by the ratio between the absorption of Si-H and Si-CH<sub>3</sub> groups, reported to the same ratio of intensities in PMHS, which was practically 1. So, the calculated CLD in DH100 was 77%. Small Si-H signals were observed in the copolymers, too, and the CLD was calculated for DH30, taking

as a reference the CoSiH30 precursor. For the remaining DH materials, the CLD cannot be calculated in the same manner, since in these cases the proportion of CH<sub>3</sub> groups is not constant.

**Table 2.** Cross-linking degrees, conversion (from FT-IR), composition details, and contact angles (CAs) of the porous materials.

Code	CLD, theor. %	Conversion, %	CLD (FT-IR), %	(CH <sub>3</sub> ) <sub>2</sub> SiO, mole %	CA, °
DH100	100	77 <sup>a</sup>	77	0	113.5 ± 3
DH70	70			30	151 ± 1
DH44	44			56	162 ± 3 (lotus)
DH30	30	39 <sup>a</sup>	11.7	70	131.5 ± 2 (petal, CAH 60°) <sup>d</sup>
DHH	72 <sup>b</sup>	84 <sup>a</sup>	55	0	124.5 ± 2
DHS	74 <sup>b</sup>	81 <sup>a</sup>	57	0	130 ± 3 (petal, CAH 51°) <sup>d</sup>
UV50	50	84 <sup>c</sup>	42	50	129 ± 2 (petal, CAH 45°) <sup>d</sup>
UVME	39	98 <sup>c</sup>	49	50	87 ± 1

<sup>a</sup> Calculated from FT-IR, as  $[(A_{2170}/A_{1260})]_{\text{final}}/[(A_{2170}/A_{1260})]_{\text{PMHS}} \times 100$ . <sup>b</sup> Representing the theoretical unmodified Si-H groups. <sup>c</sup> Calculated from FT-IR, as  $[(A_{3057}/A_{1260})]_{\text{final}}/[(A_{3057}/A_{1260})]_{\text{UV50}} \times 100$ . <sup>d</sup> Difference between CAs on the two sides of the drop at 90° tilt angle.

PHMS was chemically modified with hexene (DHH) or with allyltrimethylsilane (DHS), both hydrosilylation reactions occurring in the presence of Karstedt catalyst, simultaneously with the dehydrocoupling reaction. The long hexyl and the trimethylsilyl groups were intended to increase the hydrophobic character of the porous materials. The FT-IR spectra are shown in Figure 1, in both cases compared with DH100 as a reference. The presence of aliphatic CH<sub>2</sub> groups in DHH is proved by the adsorption bands at 2928 cm<sup>-1</sup> (asymmetric stretching vibration) and 2858 cm<sup>-1</sup> (symmetric stretching vibration) (Figure 1a). In DHS, the CH<sub>2</sub> asymmetric stretching can be seen at 2920 cm<sup>-1</sup>, while the band at 2960 (CH<sub>3</sub> asymmetric stretching vibration) is more pronounced than in DH100. In addition, two bands at 862 and 837 cm<sup>-1</sup> are assignable to Si-C stretching vibrations, one of them being due to trimethylsilyl groups [30]. The absence of a double bond absorption band, which would have appeared at around 3050 cm<sup>-1</sup>, implies that the conversion of hexene and allyltrimethylsilane was high and that the unreacted reagent was removed in the purification step. Like in the other cases, reminiscent Si-H bands still exist in both chemically modified samples. Taking PMHS as a reference, the conversion of the Si-H groups is higher than in DH100. However, two concurrent reactions occur, and part of the reacted Si-H groups is involved in cross-linking. Assuming the same conversion of Si-H groups in the cross-linking reaction, calculations indicate 28.5% modification with n-hexene (theoretical 28%) and 24% modification with ATMS (vs. 26% theoretical). Thus, we can conclude that the hexyl and propylene-trimethylsilyl groups are chemically attached to the polysiloxane backbone, and the modification reactions occurred in high yield.

An alternative set of samples was obtained by UV-photoinitiated thiol-ene addition (Scheme 1B), using a poly(dimethyl-methylvinyl)siloxane copolymer with ~50% vinyl groups, trimethylolpropane tris(3-mercaptopropionate) (SHCL) as a cross-linking agent, and 2,2-dimethoxy-2-phenylacetophenone (DMPA) as a photoinitiator (UV50). Modification of this copolymer by the addition of mercaptoethanol, occurring simultaneously with the cross-linking process, was designed to provide hydrophilicity in the resultant porous silicone (UVME). The FT-IR spectrum of UV50 showed incomplete conversion of the vinyl groups, since absorption bands at 3057 cm<sup>-1</sup> (CH stretching) and 532 cm<sup>-1</sup> (twisting vibrations) were still present. The chemical modification with mercaptoethanol resulted in the nearly complete disappearance of these bands, along with an increase in the CH<sub>2</sub> band at 2920 cm<sup>-1</sup> and in the OH band and the presence of thioether bands at 700 and 673 cm<sup>-1</sup>

(C-S-C stretching) [30] (Figure 2). The conversion and experimental CLD values in Table 2 were calculated by taking the spectrum of the initial Vi50 precursor as a reference.

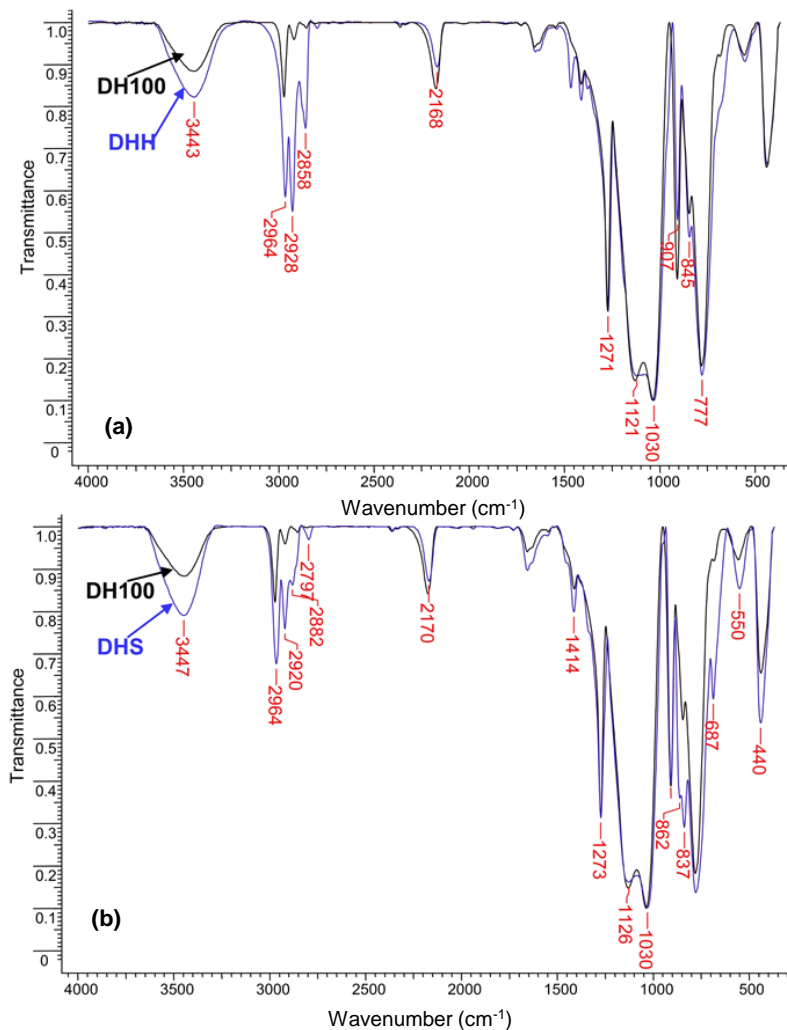


Figure 1. FT-IR spectra of DHH (a) and DHS (b) (blue lines) in comparison with DH100 (black lines).

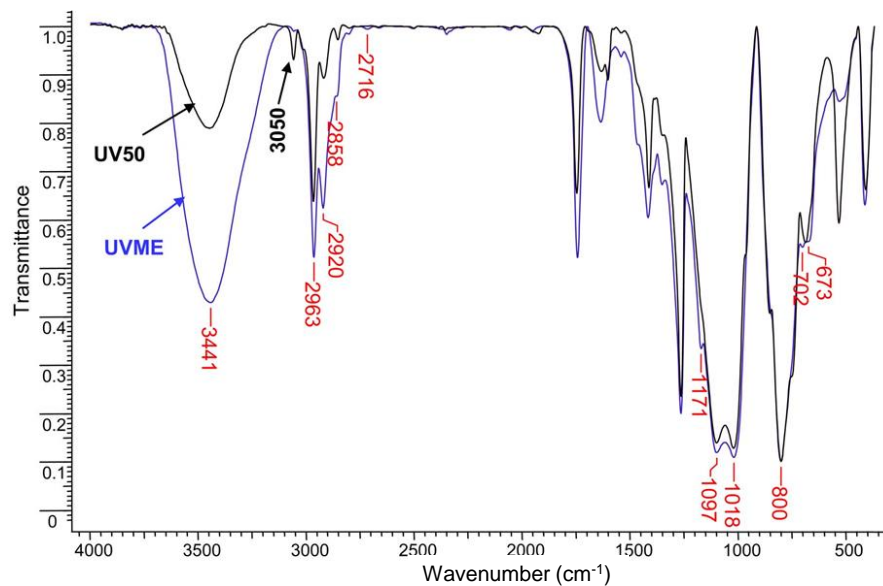
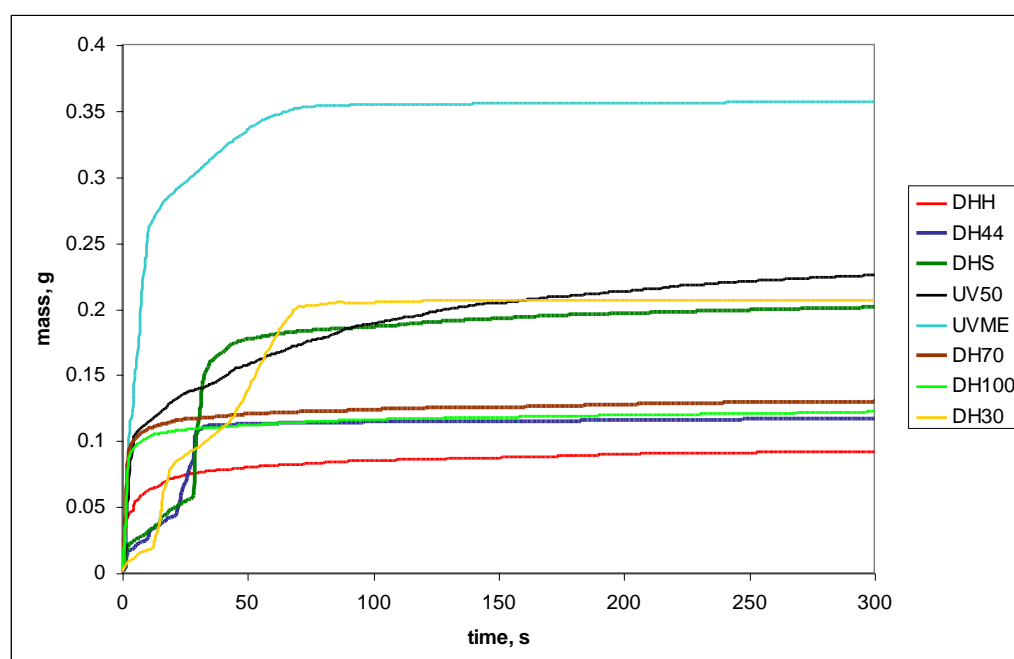


Figure 2. FT-IR spectra of UV50 (black) and UVME (blue).

The premises of the chemical modification were that, taking the polysiloxane chain as a reference, the OH groups would provide hydrophilic behavior, while dimethyl units and hexyl and trimethylsilyl groups would increase the hydrophobic behavior. Powder wetting experiments were performed in order to obtain contact angle values, but the Washburn method which was applied here has several limitations and is not suitable for hydrophobic materials [31,32]; thus, it could not be fully used as initially intended. Nevertheless, the water sorption isotherms shown in Figure 3 can be used to compare the samples. It is worth noting that all samples were packed in the same way: the same amount of powder was placed between identical pieces of filter paper. The isotherms are depicted as they were registered, without extracting the effect of the filter paper, since they are used only for comparison. The wetting experiments revealed some unexpected outcomes, and it turned out that the morphology of the materials had a significant influence on their surface properties.



**Figure 3.** Comparative water adsorption isotherms of porous silicones.

In Figure 3, the samples can be roughly divided into three categories, according to the amount of water adsorbed: below 0.12 g, around 0.2 g, and above 0.3 g. In the dehydro-coupling sample series, very little difference was registered for DH100, DH70, and DH44, although their dimethylsiloxane content increased. DH100 set the trend, being hydrophobic, in spite of some Si-OH groups being present. The other two samples containing copolymers had similar water sorption and slightly lower hexane sorption capacities (Figure S3). The sample modified with hexene (DHH) exhibited the lowest water sorption and a slightly higher affinity for hexane (Figure S3).

Unexpectedly, the water sorption capacities of the DH30 sample, with the highest content of PDMS, and the DHS modified with trimethylsilyl were significantly higher than that of the unmodified DH100, placing these in the middle range of the graph. Their sorption curves had different aspects, showing a stepwise increase before leveling. Sample UV50, which is also placed in the “middle” zone of the wetting graph, showed a very slow increase in adsorbed water after a small initial “burst”. In the attempt to verify this apparently peculiar behavior and to measure the contact angle, drops of water (ca. 10  $\mu$ L) were placed on the porous surfaces of the initial monoliths. In all these three cases, the “petal” effect was observed, i.e., a water drop did not fall off when the piece of material was tilted or even turned upside down (Supplementary Materials S2; Figure S4). This behavior is assigned to superhydrophobic materials with very high adhesion (high contact angle

hysteresis), in the so-called Cassie impregnating state [21]. In the wetting measurements, water was first adsorbed on the bottom paper layer, then it adhered to the material, filling gradually the pores. This can be seen in the slowly increasing region of the graph, which seems to characterize only the materials showing the petal effect in our experiments. The contact angle hysteresis (calculated as the difference between the CA values on the two sides of the droplet) at a 90° tilt angle (Figure S4) [19] had values of 45–60°.

It is worth mentioning that, since the samples were crushed, the observed behavior characterizes the bulk material and not necessarily the surface of the monoliths or films; thus, it could be best correlated with the morphology of the “inner” part of the materials, which will be discussed further. The static water contact angle (CA) was measured for broken samples in order to correlate the data. As for the surfaces, contact angle values could be misleading in such cases due to several effects: the migration/orientation of PDMS chains to the surface, the presence of pores larger than the water droplets, different morphologies on the two surfaces due to stratification during cross-linking [13], and so on. The apparent contact angles are summarized in Table 2. The samples exhibiting the petal effect were highly hydrophobic, with apparent CAs of around 130°, while the sample modified with ME had a CA value of 87°. Sample DHH, modified with hexyl groups, had a higher contact angle than DH100.

The CA of sample DH70 was 151°, which is at the limit of superhydrophobic materials. Sample DH44 exhibited the “lotus” effect, assigned to superhydrophobic materials with low contact angle hysteresis [21], which manifests by very low adhesion, the water droplets rolling very quickly off the surface (Supplementary Materials S3). The CA for this sample was evaluated from video captures, since the droplets rolled too quickly from the surface (estimated CAH close to 0°). This situation completes the wetting observations in correlation with the chemical structure, confirming that by introducing PDMS segments in large amounts, the hydrophobicity of the materials in fact increased compared with DH100, in spite of an apparently similar water uptake registered for the powder state. In this case, the water absorbed by the filter paper in the first seconds is repelled by the porous powder and cannot protrude between the particles to reach the second filter paper. Indeed, after the measurement, it was found out that the top layer of filter paper was dry to the touch in the case of all the samples in the lower region of the adsorption graph.

UVME showed no surprise, having the highest water adsorption capacity, since it contains hydroxyethyl groups, which are hydrophilic. In this case, the contact angle could be calculated from the powder wettability data with the Washburn method, and the obtained value was 86.8°, which is very close to that measured with the water drops.

Superhydrophobic porous silicones with CAs over 150° and low sliding angles (hysteresis) have been reported [23]. The respective materials, chemically modified at the surface with perfluoroalkyl groups, were also oleophobic (CA against *n*-decane ~121°). On the other hand, superhydrophobic and superoleophilic PDMS–MWNT sponges with very good performance in selective oil absorption have been reported [24]. The authors explained their results as a consequence of very large pores and the key role of MWCNTs being oleophilic and hydrophobic with a large surface area and a rougher surface. To our knowledge, the petal effect for highly hydrophobic porous silicones has not been reported.

The morphology of the porous samples was analyzed by SEM in cross section. In most cases, open-cell pores were observed, with particularities depending on the process and composition. In the dehydrocoupling/hydrosilylation series, the morphology was in close dependency with the composition of the reaction mixture. The material obtained from neat PMHS (DH100) had large pores due to rapid H<sub>2</sub> evolution and smaller ones which are characteristic for the materials obtained by emulsion template [13] (Figure 4a). With increasing PDMS content in the DH series, the proportion of large pores (tens of micrometers) diminished at the same observation scale, along with the decrease in the cross-linking degree of the copolymers, and practically disappeared in DH30 without the PMHS precursor (Figure 4). This trend is in agreement with experimental observations of diminished foaming and prolonged cross-linking time when the proportion of PMHS

diminished. Thus, the emulsion template had an increasing role in tuning the pore size. The generation of large pores in dehydrocoupling increased the interconnectivity of the structures, since the small pores are practically windows in the open cells; thus, hierarchical structures formed.

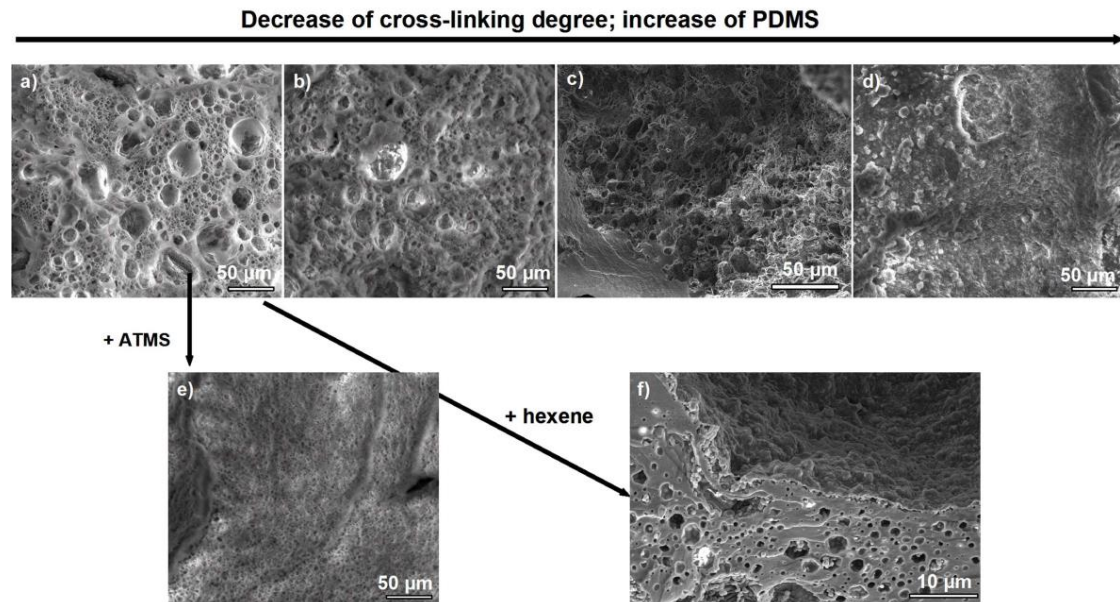


**Figure 4.** Morphology of the porous silicones in the DH series: (a) DH100, (b) DH70, (c) DH44, (d) DH30, (e) DHS, and (f) DHH.

When the PMHS was modified with ATMS, the morphology looked like a fine lace: very small pores formed almost exclusively (Figure 4e). Due to the small size, the interconnectivity of the pores could not be clearly observed in all samples. Thus, the open-cell structure was verified by immersing the samples in an acetone solution of Disperse Red 1 (DR1) for a few minutes. The pieces of porous materials were removed on a filter paper, then gently cut (or crushed). The inner parts of the materials were colored (Figure S5), which is an indication of pore interconnection [33]. When hexene was used as a modifying agent, the formation of a latex was noticed, which can be observed in the final morphology (Figure 4f) showing pores and particles.

In the absence of hydrogen evolution, the morphology of the samples obtained by photoaddition was dictated only by the emulsion template and the surface energy of the reaction mixture (Figure 5). UV50 showed fewer and interconnected pores and apparently smooth regions. A combination of particles and holes characterizes sample UVME, due to the water solubility of ME, which probably induced a combination of w/o and o/w emulsion within the reaction mixture, generating the latex.

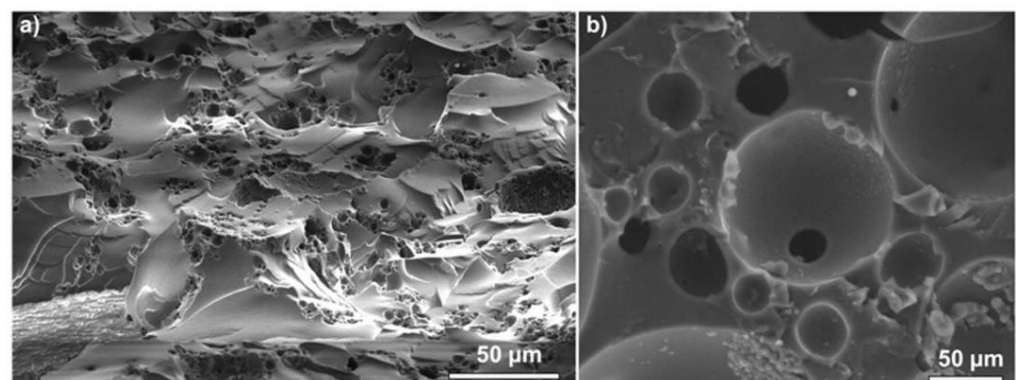


**Figure 5.** Morphology of samples obtained by photoaddition: (a) UV50 and (b) UVME.

When trying to correlate the wetting behavior with the morphology, it appears that the samples that manifested highly hydrophobic behavior with petal or lotus effects had uniformly small pores and fewer very large pores (tens of micrometers). It is well documented that such effects are generated by combinations of micro- and nanostructures; more precisely, the microstructure pitch and nanostructure density are the key parameters, but the surface energy is an important element as well [25]. It was observed that the sizes of hierarchical micro- and nanostructures are both larger in the petal than in the lotus leaf [21]. Petals from two rose species with microstructures of around 10  $\mu\text{m}$  could show different effects, depending on fine details [34]: the one with a smaller pitch value (spacing) and a larger P-B height presented a superhydrophobic surface with low adhesion. When similar microstructures and different densities of nanostructures are considered, the lower nanostructure density generates high adhesion (the petal effect) [25].

Compared with the reported examples, in our case, the effect was observed on pores and not on protuberant micro-/nanostructures, not to mention that the surface energy was modified due to changes in the chemical structure of the porous materials. When samples with similar structures (and thus surface energies) were compared at a larger scale (Figure S6), it appeared that in the case of our porous materials, the trend was somehow reversed: DH44, with larger pores, exhibited low adhesion, as compared with sample DH30, with smaller pores, which showed high adhesion. On the other hand, taking into account that the emulsion template dictated the distribution (density) of small (nano-) pores, this should be considered approximately constant in the bulk samples. When micropores are generated as a supplementary element, it results that the share of nanostructures on a microstructure is larger in materials with larger pores. Thus, in fact, when there are larger pores, there should be a higher density of nanopores on a microstructure, giving low adhesion (the case of DH44). This dual-scale porosity tunes the surface properties, similar to the dual-scale roughness [25].

Fine morphological details can be observed in Figure 6 for samples DH44 and UV50. In DH44 (showing the lotus effect), besides large pores, as seen in Figure 4c, a very high density of small (“nano”) pores of 200–500 nm was observed, with dimensions similar to the droplet sizes measured by DLS for the starting emulsion (Figure S7). These nanopores were distributed inside the larger ones, forming “windows” in the open cells. In UV50 (showing the petal effect), hierarchical, dual-scale pores were seen, of a few micrometers and around 500 nm. These areas with interconnected pores were spaced by relatively large regions without pores (Figure 5a), which could be assimilated with large pitch (spacing between microstructures).

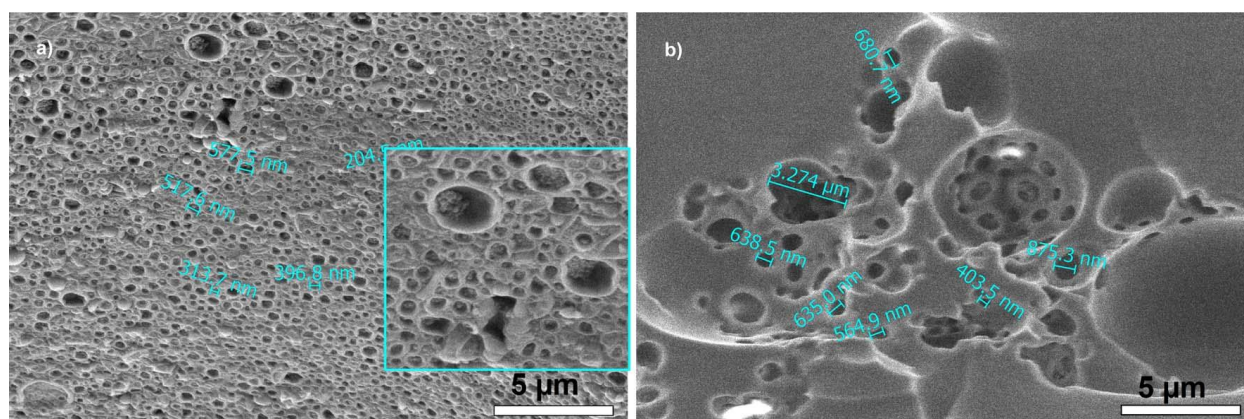


**Figure 6.** Fine morphological details of sample DH44, which exhibited the lotus effect (a), and UV50 with the petal effect (b).

Other factors have an important influence on these macroscopic effects, for example, the droplets’ size [21] or the regularity and order of hierarchical elements. In the porous materials investigated herein, the topography is rather irregular, as compared with a real

petal or leaf, and the microscopic elements have roughly one order smaller dimensions. The water droplet size was ca. 10  $\mu\text{L}$ , similar as in other studies [21], in order to prevent the evaporation effect, since it was established that the use of a drop volume of up to 10 microliters has no influence on water static contact angle values [35]. One should also consider the hydrophobic nature of the bulk materials, in addition to the induced porosity.

The as-obtained DH materials did not show good mechanical properties, due to the large pores and thin walls, and some of them were crushed during manipulation. In the case of photoaddition reaction, UV50 was a more robust material, with a certain flexibility. This correlates with the morphology of this sample, which showed large smooth areas (very thick walls of the pores). Selected samples were measured in compression stress–strain tests and gave the following Young’s modulus values: 45.5 kPa for DH100, 561 kPa for DH70, and 395 kPa for UV50.

#### 4. Conclusions

In this contribution, we showed a simple way of tuning the inner surface properties of porous silicone materials obtained from in-house prepared precursors with various chemical structures. Although porous silicones with fine performances have been reported, most of them were obtained from commercial kits without chemical modifications, while their surface properties were rarely investigated.

By combining chemical structure variations and the emulsion template preparation method, fine-tuning of the surface properties of porous hydrophobic silicones was observed. The materials were obtained by cross-linking reactions occurring in emulsion generated with a siloxane surfactant, i.e., dehydrocoupling or thiol-ene photoaddition reactions, in mild conditions. The porosity decreased along with the cross-linking degree in the dehydrocoupling series, while morphological particularities dictated peculiar surface properties. Chemical modification in situ of poly(methylhydrogen)siloxane with hexene or allyltrimethylsilane successfully further increased the hydrophobicity, while the addition of mercaptoethanol to a poly(dimethyl-methylvinyl)siloxane copolymer produced a hydrophilic porous silicone. The powder wetting experiments, correlated with visual observations and contact angle measurements, revealed the essential role of morphology, besides chemical structure, in tuning the surface properties of these porous materials. Most of the samples were highly hydrophobic, exhibiting either superhydrophobic lotus or rose petal effects. The latter case in particular is rarely discussed in similar materials.

**Supplementary Materials:** The following supporting information can be downloaded at: <https://www.mdpi.com/article/10.3390/app131910899/s1>, Figure S1: Water/toluene emulsion ( $f = 0.5$ ) before (a) and after two hours at 50 °C (b); Figure S2: FT-IR spectra of DH44 (blue) and DH100 (black); Figure S3: Hexane sorption isotherms; Figure S4: The petal effect on porous samples; Figure S5: Samples stained with DR1 acetone solution (acetone is a non-solvent for the silicone materials): after a few minutes the inner surface of the samples is obviously colored, as compared with the non-stained pieces of material; Figure S6: Comparison of large scale morphology of sample DH44 with lotus effect and DH30 with petal effect; Figure S7: DLS analysis of the emulsion template (water in toluene,  $f = 0.5$ ); Video S1: The petal effect; Video S2: The lotus effect.

**Author Contributions:** Conceptualization, C.R.; Methodology, C.R. and A.-L.V.; Validation, C.R.; Investigation, C.R. and A.-L.V.; Data Curation, C.R. and A.-L.V.; Writing—Original Draft Preparation, C.R.; Writing—Review and Editing, C.R. and A.-L.V. All authors have read and agreed to the published version of the manuscript.

**Funding:** This research received no external funding.

**Data Availability Statement:** Data will be made available on request.

**Acknowledgments:** The authors express their gratitude to Adrian Bele for mechanical tests.

**Conflicts of Interest:** The authors declare no conflict of interest.

## References

1. Mudassir, M.A.; Aslam, H.Z.; Ansari, T.M.; Zhang, H.; Hussain, I. Fundamentals and Design-Led Synthesis of Emulsion-Templated Porous Materials for Environmental Applications. *Adv. Sci.* **2021**, *8*, 2102540. [[CrossRef](#)] [[PubMed](#)]
2. Kramer, S.; Cameron, N.R.; Krajnc, P. Porous Polymers from High Internal Phase Emulsions as Scaffolds for Biological Applications. *Polymers* **2021**, *13*, 1786. [[CrossRef](#)] [[PubMed](#)]
3. Cazacu, M.; Dascalu, M.; Stiubianu, G.-T.; Bele, A.; Tugui, C.; Racles, C. From passive to emerging smart silicones. *Rev. Chem. Eng.* **2022**, *39*, 941–1003. [[CrossRef](#)]
4. Racles, C.; Dascalu, M.; Bele, A.; Cazacu, M. Reactive and Functional Silicones for Special Applications. In *Reactive and Functional Polymers Volume One*; Gutiérrez, T.J., Ed.; Springer: Cham, Switzerland, 2020; pp. 235–292. [[CrossRef](#)]
5. Yan, H.; Wang, K.; Zhao, Y. Fabrication of Silicone Rubber Foam with Tailored Porous Structures by Supercritical CO<sub>2</sub>. *Macromol. Mater. Eng.* **2017**, *302*, 1600377. [[CrossRef](#)]
6. Masihi, S.; Panahi, M.; Maddipatla, D.; Hanson, A.J.; Bose, A.K.; Hajian, S.; Palaniappan, V.; Narakathu, B.B.; Bazuin, B.J.; Atashbar, M.Z. Highly Sensitive Porous PDMS-Based Capacitive Pressure Sensors Fabricated on Fabric Platform for Wearable Applications. *ACS Sens.* **2021**, *6*, 938–949. [[CrossRef](#)]
7. Choi, S.J.; Kwon, T.H.; Im, H.; Moon, D.I.; Baek, D.J.; Seol, M.L.; Duarte, J.P.; Choi, Y.K. A Polydimethylsiloxane (PDMS) Sponge for the Selective Absorption of Oil from Water. *ACS Appl. Mater. Interfaces* **2011**, *3*, 4552–4556. [[CrossRef](#)]
8. Zimny, K.; Merlin, A.; Ba, A.; Aristégui, C.; Brunet, T.; Mondain-Monval, O. Soft porous silicon rubbers as key elements for the realization of acoustic metamaterials. *Langmuir* **2015**, *31*, 3215–3221. [[CrossRef](#)]
9. Si, J.; Cui, Z.; Xie, P.; Song, L.; Wang, Q.; Liu, Q.; Liu, C. Characterization of 3D elastic porous polydimethylsiloxane (PDMS) cell scaffolds fabricated by VARTM and particle leaching. *J. Appl. Polym. Sci.* **2016**, *133*, 42909–42917. [[CrossRef](#)]
10. Zhao, J.; Chen, H.; Ye, H.; Zhanga, B.; Xu, L. Poly(dimethylsiloxane)/graphene oxide composite sponge: A robust and reusable adsorbent for efficient oil/water separation. *Soft Matter* **2019**, *15*, 9224–9232. [[CrossRef](#)]
11. Abshirini, M.; Saha, M.C.; Cummings, L.; Robison, T. Synthesis and characterization of porous polydimethylsiloxane structures with adjustable porosity and pore morphology using emulsion templating technique. *Polym. Eng. Sci.* **2021**, *61*, 1943–1955. [[CrossRef](#)]
12. Pruvost, M.; Smit, W.J.; Monteux, C.; Poulin, P.; Colin, A. Polymeric foams for flexible and highly sensitive low-pressure capacitive sensors. *NPJ Flex. Electron.* **2019**, *3*, 7. [[CrossRef](#)]
13. Racles, C.; Bele, A.; Vasiliu, A.-L.; Sacarescu, L. Emulsion Gels as Precursors for Porous Silicones and All-Polymer Composites—A Proof of Concept Based on Siloxane Stabilizers. *Gels* **2022**, *8*, 377. [[CrossRef](#)] [[PubMed](#)]
14. Shao, Y.; Luo, C.; Deng, B.W.; Yin, B.; Yang, M.-B. Flexible porous silicone rubber-nanofiber nanocomposites generated by supercritical carbon dioxide foaming for harvesting mechanical energy. *Nano Energy* **2020**, *67*, 104290–104296. [[CrossRef](#)]
15. Brook, M.A. New Control Over Silicone Synthesis using SiH Chemistry: The Piers–Rubinsztajn Reaction. *Chem. Eur. J.* **2018**, *24*, 8458–8469. [[CrossRef](#)]
16. Kobayashi, T.; Saitoh, H.; Fujii, N.; Hoshino, Y.; Takanashi, M. Porous Membrane of Polydimethylsiloxane by Hydrosilylation Cure: Characteristics of Membranes Having Pores Formed by Hydrogen Foams. *J. Appl. Polym. Sci.* **1993**, *50*, 971–979. [[CrossRef](#)]
17. Mizerska, U.; Fortuniak, W.; Rubinsztajn, S.; Chojnowski, J. Impact of cross-linker on the structure and hydrophilic–hydrophobic properties of polyhydromethylsiloxane-derived microspheres. *Polym. Adv. Technol.* **2021**, *32*, 3967–3974. [[CrossRef](#)]
18. Wang, Z.H.; Liu, X.Y.; Zhang, H.Q.; Wang, Y.; Xu, Y.F.; Peng, B.L.; Liu, Y. Modeling of kinetic characteristics of alkaline-surfactant-polymer-strengthened foams decay under ultrasonic standing wave. *Pet. Sci.* **2022**, *19*, 1825–1839. [[CrossRef](#)]
19. Eral, H.B.; Mannetje, D.J.C.M.; Oh, J.M. Contact angle hysteresis: A review of fundamentals and applications. *Colloid Polym. Sci.* **2013**, *291*, 247–260. [[CrossRef](#)]
20. Liu, Y.; Choi, C.-H. Condensation-induced wetting state and contact angle hysteresis on superhydrophobic lotus leaves. *Colloid Polym. Sci.* **2013**, *291*, 437–445. [[CrossRef](#)]
21. Feng, L.; Zhang, Y.; Xi, J.; Zhu, Y.; Wang, N.; Xia, F.; Jiang, L. Petal Effect: A Superhydrophobic State with High Adhesive Force. *Langmuir* **2008**, *24*, 4114–4119. [[CrossRef](#)] [[PubMed](#)]
22. Li, Z.; Wang, X.; Bai, H.; Cao, M. Advances in Bioinspired Superhydrophobic Surfaces Made from Silicones: Fabrication and Application. *Polymers* **2023**, *15*, 543. [[CrossRef](#)]
23. Cao, J.; Wang, D.; Wang, L.; Feng, S.A. Superhydrophobic and Oleophobic Silicone Sponge with Hierarchical Structures. *Macromol. Rapid Commun.* **2021**, *42*, 2000761–2000767. [[CrossRef](#)]
24. Turco, A.; Malitesta, C.; Barillaro, G.; Greco, A.; Maffezzolic, A.; Mazzotta, E. A magnetic and highly reusable macroporous superhydrophobic/superoleophilic PDMS/MWNT nanocomposite for oil sorption from water. *J. Mater. Chem. A* **2015**, *3*, 17685–17696. [[CrossRef](#)]
25. Ebert, D.; Bhushan, B. Wear-resistant rose petal-effect surfaces with superhydrophobicity and high droplet adhesion using hydrophobic and hydrophilic nanoparticles. *J. Colloid Interface Sci.* **2012**, *384*, 182–188. [[CrossRef](#)]
26. Racles, C.; Alexandru, M.; Musteata, V.; Bele, A.; Cazacu, M.; Opris, D.M. Tailoring the dielectric properties of silicones by chemical modification. In *Recent Research Developments in Polymer Science*; Pandalai, S.G., Ed.; Transworld Research Network: Trivandrum, India, 2014; Volume 12, pp. 17–36. ISBN 978-81-7895-611-4.
27. Cazacu, M.; Marcu, M.; Holerca, M.N.; Petrovan, S.; Lazarescu, S. Heterogeneous catalyzed copolymerization of octamethylcyclotetrasiloxane with 1,3,5,7-tetramethyl-1,3,5,7-tetramethylcyclotetrasiloxane. *J. Macromol. Sci. Pure Appl. Chem. A* **1996**, *33*, 65–76. [[CrossRef](#)]

28. Racles, C.; Sillion, M.; Sacarescu, L. Multi-tasking pyridyl-functionalized siloxanes. *Colloids Surf. A Physicochem. Eng. Asp.* **2018**, *547*, 102–110. [[CrossRef](#)]
29. Lamour, G.; Hamraoui, A.; Buvailo, A.; Xing, Y.; Keuleyan, S.; Prakash, V.; Eftekhari-Bafrooei, A.; Borguet, E. Contact Angle Measurements Using a Simplified Experimental Setup. *J. Chem. Educ.* **2010**, *87*, 1403–1407. [[CrossRef](#)]
30. Socrates, G. *Infrared and Raman Characteristic Group Frequencies: Tables and Charts*, 3rd ed.; John Wiley & Sons: Chichester, UK, 2004; pp. 1–368.
31. Kirdponpattara, S.; Phisalaphong, M.; Zhang Newby, M. Applicability of Washburn capillary rise for determining contact angles of powders/porous materials. *J. Colloid Interface Sci.* **2013**, *397*, 169–176. [[CrossRef](#)] [[PubMed](#)]
32. Spagnolo, D.A.; Maham, Y.; Chuang, K.T. Calculation of Contact Angle for Hydrophobic Powders Using Heat of Immersion Data. *J. Phys. Chem.* **1996**, *100*, 6626–6630. [[CrossRef](#)]
33. Zhang, T.; Xu, Z.; Guo, Q. Closed-cell and open-cell porous polymers from ionomer-stabilized high internal phase emulsions. *Polym. Chem.* **2016**, *7*, 7469–7476. [[CrossRef](#)]
34. Bhushan, B.; Her, E.K. Fabrication of Superhydrophobic Surfaces with High and Low Adhesion Inspired from Rose Petal. *Langmuir* **2010**, *26*, 8207–8217. [[CrossRef](#)] [[PubMed](#)]
35. Effect of Drop Volume on Static Contact Angles, Spyridon Kranias, Technical Note 310e, Krüss GmbH. Available online: [https://warwick.ac.uk/fac/cross\\_fac/sciencecity/programmes/internal/themes/am2/booking/dropshapeanalyser/effect\\_of\\_drop\\_volume\\_on\\_static\\_contact\\_angles.pdf](https://warwick.ac.uk/fac/cross_fac/sciencecity/programmes/internal/themes/am2/booking/dropshapeanalyser/effect_of_drop_volume_on_static_contact_angles.pdf) (accessed on 2 September 2023).

**Disclaimer/Publisher’s Note:** The statements, opinions and data contained in all publications are solely those of the individual author(s) and contributor(s) and not of MDPI and/or the editor(s). MDPI and/or the editor(s) disclaim responsibility for any injury to people or property resulting from any ideas, methods, instructions or products referred to in the content.